IV. SUMMARY

We have emphasized the role of the surroundings in the form factors of an ion. When they change, as they do on alloying, Harrison's recipe is too inadequate to take into account the effect of their change because of the accompanying changes in the Fermi momentum, the position of the zero of the energy in the crystal relative to that for the free ion, and the orthogonalization charge. These can be taken into account only by doing the whole calculation all over again: No short-cut appears to be available. The results of such a calculation are found to give a considerably better agreement than obtained by Harrison except for the alloy Al in Mg. That our results for the alloys obtained from the combinations of Li, Na, and K differ considerably from those of Dickey *et al.* should not be disturbing, in view of the large divergences between the experimental values for the resistivities of (pure) liquid Li, Na, and K and those obtained from the MNY phase shifts employed by Dickey *et al.* It will be of interest to have the experimental results for these alloys.

ACKNOWLEDGMENTS

The author is grateful to Professor A. B. Bhatia for guidance and helpful discussions. Thanks are due to Professor W. A. Harrison and Dr. A. O. E. Animalu for very useful correspondence. Thanks are also due to Dr. K. C. Sharma and C. J. Elliott for assistance in computing.

PHYSICAL REVIEW VOLUME 174, NUMBER 3 15 OCTOBER 1968

Fermi Surface of Cadmium: Radio-Frequency Size Effect*

R. C. JONES,† R. G. GOODRICH, AND L. M. FALICOV‡
Department of Physics, Louisiana State University, Baton Rouge, Louisiana
(Received 14 August 1967; revised manuscript received 3 June 1968)

The Fermi of cadmium is determined from calipers obtained through rf size-effect measurements. The 6- to 8-MHz rf measurements were performed at 1.2°K on high-purity monocrystals of cadmium approximately 0.5 mm in thickness. The Fermi surface was calipered using samples whose normals to the surfaces were parallel to one of the three principal symmetry directions [0001], [10$\bar{1}$0], and [11$\bar{2}$0], with magnetic field rotations in the plane of the sample. Calipers are assigned to definite orbits on the first- and second-band hole surfaces and the third-band electron surface. The third-band electron "lens" is found to be smooth and round with a major diameter of 1.560 Å^{-1} and varying less than 1% in the basal plane. The minor diameter has a caliper of 0.556 Å^{-1}. Calipers are given for the first-band hole surface except near its pointed ends. The second-band hole surface is discussed in detail with the assignment of 17 series of calipers to definite orbits on this sheet of the Fermi surface. Both the first and second bands of holes are found to have considerably smaller cross sections than predicted by the single-orthogonalized-plane-wave construction. Detailed comparisons to a recent pseudopotential calculation of the energy bands and the Fermi surface are made. No calipers were observed that could be assigned to the third-band "stars" or the fourth-band electron "cigars."

I. INTRODUCTION

IN the last ten years rapid progress has been made in developing experimental techniques for obtaining information about the electronic structure of metals. From all of the experimental methods that have been tried, four techniques have evolved which give the most direct information about the size and shape of the Fermi surface (FS) of metals. Of these four techniques, perhaps the most widely used has been the de Haas–van Alphen (dHvA) effect. In observing the dHvA and other closely related effects, one measures the influence of the quantization of the electronic states in a magnetic field on either the magnetic susceptibility or upon various transport properties of the metals as these states pass through the Fermi level with increasing magnetic field. Values of the extremal areas of the various sheets of the FS are deduced from the periodic variation of these properties as the magnetic field is increased. The technique suffers from the difficulty of trying to separate the many different periods that may be observed in more complicated metals and from the fact that only the area and not the shape of a particular section of the FS can be obtained. The salient virtue of the technique, however, is that it does not require, in general, as long a mean free path of the carriers as do the other techniques.

The rate of change of area of a cross section of the FS with respect to energy, evaluated at the Fermi energy, can be obtained through cyclotron-resonance measurements. Once both the area and its derivative with respect to energy are known, in principle the FS can be constructed, but in practice this is a very difficult procedure. The cyclotron-resonance experiments suffer

* Work supported by the U. S. Atomic Energy Commission; AEC Report No. ORO-3087-28.
† Present address: Department of Physics, University of California, Riverside, Calif.
‡ Permanent address: James Franck Institute and Department of Physics, The University of Chicago, Chicago, Ill.

from the rather stringent conditions placed on the preparation of samples and from the fact that the frequency of scattering of the carriers must be much less than the frequency of the radiation applied to observe the resonance.

A much more direct method of determining the size and shape of the FS is to caliper it across its extremal dimensions. There are two techniques available for doing this. The first effect to be investigated was the oscillatory change in the attenuation of ultrasound propagating in a sample subjected to an increasing magnetic field applied perpendicular to the direction of propagation of the sound wave. A period in the oscillatory attenuation is completed every time a diameter of an extremal orbit of carriers on the FS becomes equal to a multiple of the wavelength of the ultrasound. In order to observe this geometric resonance, the mean free path of the carriers must be long compared with the acoustic wavelength, and the gross acoustic attenuation must be small so that the small oscillatory changes can be observed. As in both the de Haas–van Alphen and cyclotron-resonance techniques, the information that is available from the geometric-resonance data depends upon the ability to separate many periodic oscillations superimposed upon one another.

The remaining technique for determining extremal dimensions of the FS is the radio-frequency size effect (RFSE) first reported by Gantmakher,[1] and the application of this technique to cadmium is the subject of the remainder of this paper. Experimentally, the RFSE consists of observing singularities in the surface impedance of a thin single-crystalline slab placed in a magnetic field that is imposed parallel to the faces of the sample. At magnetic field strengths such that an extremal cyclotron orbit of a carrier spans the sample thickness, a singularity in the surface impedance of the sample is observed. The magnetic field strength at which the singularity occurs for a given sample thickness is directly proportional to an extremal dimension of the FS. Since subharmonic signals do not occur in this case, the data are, in principle, easy to analyze; however, the technique is limited to very pure metals in which the mean free path can be made several times the thickness of the samples.

The FS of cadmium has been studied by both of the above-mentioned techniques. Several dHvA measurements have been performed, the most recent of which are by Grassie[2] and by Tsui and Stark.[3] Cyclotron-resonance measurements have been performed by Galt *et al.*[4] and by Shaw *et al.*[5] Some calipers of the FS have been obtained from the geometric resonance of Gibbons and Falicov,[6] of Daniel and Mackinnon,[7] and of Chang[8] and from the RFSE measurements of Naberezhnykh *et al.*[9] Only as a result of the present investigation have extensive calipers for field rotations in the basal plane become available.[10]

The results of all of the above experimental investigations have established that the FS of cadmium differs from the free-electron surface obtained from the single orthogonalized-plane-wave (OPW) construction of Harrison[11] in certain important aspects. The experimental dimensions of the surface are considerably smaller than predicted by the single-OPW construction, and degeneracies at certain points in the Brillouin zone (BZ) are removed by the effects of finite spin-orbit coupling. Recently, Stark and Falicov[12] (SF) have calculated the electronic band structure of both zinc and cadmium, using an empirical, nonlocal pseudopotential scheme that includes spin-orbit effects. These calculations show excellent agreement with the extremal areas measured by the dHvA effect and, as will be shown herein, with the shape of the FS as obtained from the RFSE.

In the sections which follow, first a discussion of the free-electron FS for cadmium and the modification as calculated by SF is given; it is followed by a general discussion of the RFSE and the details of the present experimental technique. The last two sections present the data, their interpretation, and comparison with the calculation of SF.

II. THEORY

A. Fermi Surface of Cadmium

Cadium is a divalent metal (atomic number 48) that forms an hcp lattice; the low-temperature lattice paramaters are $a=2.9684$ Å and $c=5.5261$ Å.[9] The BZ for cadmium is shown in Fig. 1, and the distances between pairs of points are $\Gamma A=0.569$ Å^{-1}, $\Gamma M=1.222$ Å^{-1}, and $\Gamma K=1.411$ Å^{-1}. The radius of the free-electron Fermi sphere is $k_F=1.407$ Å^{-1}. Experimental work on several polyvalent metals has shown that in order to obtain an experimental picture of the FS of a metal it is necessary to start from some approximate theoretical model that can be suitably modified to agree with the experi-

[1] V. F. Gantmakher, Zh. Eksperim. i Teor. Fiz. **42**, 1416 (1962); **43**, 345 (1962); **44**, 811 (1963) [English transls.: Soviet Phys.—JETP **15**, 982 (1962); **16**, 247 (1962); **17**, 549 (1963)]; V. F. Gantmakher and E. A. Kaner, Zh. Eksperim. i Teor. Fiz. **45**, 1430 (1963) [English transl.: Soviet Phys.—JETP **18**, 988 (1964)]; V. F. Gantmakher and I. P. Krylov, Zh. Eksperim. i Teor. Fiz. **49**, 1054 (1965) [English transl.: Soviet Phys.—JETP **22**, 734 (1966)]; I. P. Krylov and V. F. Gantmakher, Zh. Eksperim. i Teor. Fiz. **51**, 740 (1966) [English transl.: Soviet Phys.—JETP **24**, 492 (1967)].

[2] A. D. C. Grassie, Phil. Mag. **9**, 847 (1964).

[3] D. C. Tsui and R. W. Stark, Phys. Rev. Letters **16**, 19 (1966).

[4] J. K. Galt, F. R. Merritt, and J. N. Klauder, Phys. Rev. **139**, A823 (1965).

[5] M. P. Shaw, T. G. Eck, and D. A. Zych, Phys. Rev. **142**, 407 (1966).

[6] D. F. Gibbons and L. M. Falicov, Phil. Mag. **8**, 117 (1963).

[7] M. R. Daniel and L. Mackinnon, Phil. Mag. **8**, 537 (1963).

[8] F. H. S. Chang, Ph.D. dissertation, The University of Texas, 1966 (unpublished).

[9] V. P. Naberezhnykh, A. A. Mar'Yakhin, and V. L. Mel'Nik, Zh. Eksperim. i Teor. Fiz. **52**, 617 (1967) [English transl.: Soviet Phys.—JETP **25**, 403 (1967)].

[10] R. G. Goodrich and R. C. Jones, Phys. Rev. **156**, 745 (1967).

[11] W. A. Harrison, Phys. Rev. **118**, 1190 (1960).

[12] R. W. Stark and L. M. Falicov, Phys. Rev. Letters **19**, 795 (1967).

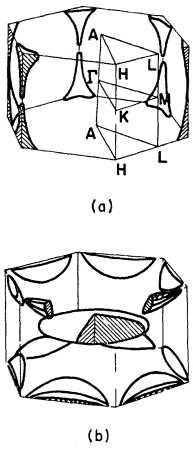

FIG. 1. Portion of the nearly-free-electron FS for cadmium: (a) first-band holes (caps); (b) third-band electron (lens and stars) and forth-band electron (cigars)—cross-hatched.

mental information. For this reason, the single-OPW construction of Harrison, with some of the known modifications due to spin-orbit coupling, is shown in Figs. 1 and 2. The first band contains only two small pockets of holes ("caps") about the point H in the BZ. The first band is separated by spin-orbit splitting from the main region of holes existing in the second band. The second band, usually called the "monster," consists of two independent sheets, related to each other by symmetry; each one of these sheets is connected to itself in the KH direction. The third band (electrons) contains one large central pocket around Γ ("lens"); the single-OPW construction predicts additional sheets ("stars") around each of the three L points. The calculation of SF, however, shows that both these third-band star pieces of the FS and the corresponding fourth-band electron sections ("cigars") predicted by the single-OPW construc- are not present in cadmium. The free-electron construction predicts that the second-band sheets are connected to each other by a small region that goes across the ΓM line; this region is shown pinched off here because of lack of evidence of a connected orbit in the dHvA as well as in magnetoacoustic experiments by several workers[13,14]; this feature is also predicted by SF.

B. Radio-Frequency Size Effect

In the presence of an applied magnetic field $\mathbf{H}$, the carriers in a metal move in reciprocal space on the FS in planes perpendicular to the direction of $\mathbf{H}$. The projections of the real-space orbits that result from this motion onto a plane perpendicular to $\mathbf{H}$ have the same shape as the orbits in reciprocal space but are rotated 90° about $\mathbf{H}$. The relation between a dimension $\mathbf{K}$ in reciprocal space and the corresponding dimension $\mathbf{r}$ in real space is given as

$$\hbar\mathbf{K}=(e/c)\mathbf{H}\times\mathbf{r}, \tag{1}$$

where $\hbar$ is Planck's constant divided by 2π, e is the electronic charge, and c is the velocity of light. Thus if a real-space dimension of an electron orbit is given at a known magnetic field, the corresponding orbit dimension in reciprocal space can be determined.

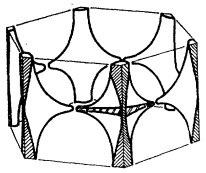

FIG. 2. Second-band hole surface for cadmium (monster) according to the nearly-free-electron theory.

If a thin flat single crystal of metal is placed in a coil carrying an rf current of angular frequency ω, then there is induced in the metal an electromagnetic field near the surfaces that extends into the metal to a depth δ (the skin depth). If the frequency ω is high enough so that $\delta\ll d$ (the sample thickness), and yet low enough so that $\omega\ll\Omega=eH/m^*c$, where m^* is the effective mass and Ω is the cyclotron frequency of the carriers, then the carriers experience a nearly static electric field near the surfaces of the sample. That is, the electrons complete many cyclotron orbits and are scattered before the field changes appreciably. At magnetic field strengths such that carriers on the FS having orbits with reciprocal-space extremal dimensions in the direction of $\mathbf{n}\times\mathbf{H}$ (where $\mathbf{n}$ is the unit vector normal to the sample surfaces) span the sample thickness, a discontinuity in the surface impedance occurs. The discontinuity arises from the relatively large increase in the number of carriers whose real-space orbits pass through the skin layer on both of the sample faces. At lower magnetic field strengths, the carriers strike the surface and cannot complete an entire orbit; at higher fields they cannot pass simultaneously through the skin layers on both surfaces.

Experimentally the magnetic field strength H is measured at the point of discontinuity in the surface impedance of a sample of known thickness d; then an extremal diameter k_c of the FS can be calipered using the relation

$$k_c=(e/\hbar c)Hd=0.015194Hd, \tag{2}$$

where k_c is in Å^{-1}, H is in G, and d is in mm.

Kaner and Fal'ko[15] have given a theory for the line shapes encountered in the RFSE. Their calculation predicts two distinct types of line shapes, one for a minimum and the other for a maximum caliper. Orbits were encountered in the present investigation that should have produced both of these line shapes; however, the agreement with predicted shapes was not good and a definite assignment to maximum and minimum calipers could not be made from the line shapes. In the present investigation, the geometry of the experimental arrangement was different from that assumed in the theory: A bilateral rf excitation was employed rather than a unilateral one, and also the rf coil axis was generally not

[13] W. A. Harrison, Phys. Rev. **126**, 497 (1962).
[14] T. G. Berlincourt, Phys. Rev. **94**, 1172 (1954).
[15] E. A. Kaner and V. L. Fal'ko, Zh. Eksperim. i Teor. Fiz. **51**, 586 (1966) [English transl.: Soviet Phys.—JETP **24**, 392 (1967)].

parallel to the applied magnetic field. The theory also assumes only circular orbits, which is not the case in Cd.

III. EXPERIMENT

A. Sample Preparation

The samples used in this experiment were cut from a zone-refined bar of cadmium obtained from Cominco Products Inc. (quoted purity: 99.9999%). A portion of this bar was etched in 30% fuming nitric acid and 70% glacial acetic acid for 1 min so that the boundaries between the crystals could be observed. A large crystal was then selected and cut from the bar by spark erosion, using a tungsten wire as the cutting tool. The resulting monocrystal was oriented by Laue back-reflection x-ray photographs, and a slab approximately 3 mm thick was cut from the crystal. Slabs cut in this manner had normals to their surfaces nearly parallel to one of the three principal symmetry directions ([0001], $[10\bar{1}0]$, or $[11\bar{2}0]$).

Since the opposite faces of the finished samples need to be as parallel as possible, the following technique was developed that gives a high degree of parallelism. The spark cutter is equipped with a planing wheel that can be used to obtain flat surfaces. This planing wheel was first checked for flatness in a lathe, using a precision indicator. It was then mounted on the servo arm of the spark cutter and not moved for the duration of the sample preparation. The arm on which the goniometer was mounted in the spark cutter was also fixed in position with marks placed on the arm so that the goniometer could be removed and replaced in exactly the same position. An aluminum block of slightly larger area than the cadmium slab was glued (using silver paint) to the goniometer to be used as a mount for the final planing of the sample. Aluminum was used because it is itself readily planed. The goniometer was set in the (0°,0°) position which made the table approximately parallel to the planing wheel, and the upper surface of the aluminum block was planed flat, resulting in a mounting surface parallel to the planing wheel. The previously cut slab of cadmium was glued to the surface of the aluminum block, and the desired principal axis was aligned parallel to the known direction of an x-ray beam with as great an accuracy as possible (±1°). The goniometer was again mounted in the spark cutter and one side of the cadmium was planed flat. Following this, the specimen was removed from the aluminum block and turned over so that the flat surfaces of the aluminum and the flat aligned surface of the cadmium were placed together. Care was taken when gluing the cadmium back to the aluminum to ensure that no silver paint ran between the two flat surfaces causing misalignment. The goniometer was then returned to the (0°,0°) position and the specimen was planed to the desired thickness.

Samples obtained with the above procedure were typically 20×30×0.5 mm. These slabs were then dipped in a solution of 75% fuming nitric acid and 25% water at 0°C. This polish removes the thin layer of spark damage on the surface, but because of the large surface-to-volume ratio of these slabs it was necessary to polish only for short periods, since the acid around the sample quickly came to a boil. The polishing time was usually about 1 sec and then the slab was quickly dipped in water. The surfaces obtained in this manner were shiny, but not mirrorlike.

Samples of 5×5 mm were then cut by spark erosion from the central portion of the slab. The edges of the large slab were discarded because of possible rounding of the corners during the polishing procedure. The orientations of these finished samples were again checked and the normals to the faces were always found to be within 1° of arc of the desired crystallographic axis.

Since one of the two experimental parameters is the thickness of the sample, it must be determined as accurately as possible. The most satisfactory procedure for this measurement was found to be to measure the larger dimensions of the sample with a traveling microscope so that the surface area of the parallel faces could be computed, and then to weigh the sample to determine its mass; from the known density of cadmium the thickness d could be determined. This procedure gives the average thickness very accurately at room temperature, but the thickness at 1°K must be known, since all of the magnetic-field measurements were performed at that temperature. The thermal-expansion data of Grüneisen and Goens[16] give the following dimensional change in cadmium from 1 to 293°K:

$$\|[0001],\ 1.38\%,\ \text{and}\ \perp[0001],\ 0.40\%.$$

These corrections were applied to determine d for the calculation of k_c values from critical-magnetic-field measurements.

The resistivity ratio was measured on a larger sample and was found to be $\rho_{300°K}/\rho_{4.2°K}=20\,800$. The size-effect peaks became about 20 times more intense upon reducing the temperature from 4.2 to 2°K, at which point no further increase in amplitude was observed.

B. Experimental Apparatus

The sample was placed on a thin piece of mica which supported it during the experiment, and a flat coil of No. 45 copper wire was wound around both the sample and the mica support. Care was exercised to have the sample occupy as much of the cross-sectional area of the coil as possible. This coil formed part of the resonant circuit of a marginal oscillator[17] operating from 6 to 8 MHz. This range of frequencies was selected because it satisfied the conditions for the RFSE: $\delta \ll d$ and $\omega \ll \Omega$. The coil and sample were immersed in liquid He^4 inside a conventional double Dewar system (see Fig. 3) and the temperature was reduced to 1.2°K by pumping.

[16] E. Grüneisen and E. Goens, Z. Physik **29**, 141 (1924).
[17] W. D. Knight, Rev. Sci. Instr. **32**, 95 (1961).

The magnetic field was supplied by a small iron-core magnet that could be rotated in the horizontal plane of the sample. The angle that the magnetic field formed with one of the crystallographic axes of the sample could be set within $\pm 0.1°$ and could be determined to within 0.5° from the symmetry of the data. During a run the angle of the magnet was rotated 30° on either side of the axis of the rf coil; thus it was necessary to remove the sample and rewind the coil to cover the full 90° between axes for two of the sample orientations. A transistorized power supply was constructed for the magnet that had the capability of sweeping the magnet current through zero and applying a small current in the reverse direction so that the residual field of approximately 30 G could be cancelled to obtain low fields. A Hall probe, which was calibrated in place with an NMR gaussmeter, was used to measure the magnetic field. During a sweep of the magnetic field, markers were placed on the recording to calibrate each trace.

A pair of modulation coils was wound on plastic forms and mounted on the iron pole pieces of the magnet to provide an ac amplitude modulation of the applied magnetic field. A frequency of 40 Hz was selected for the amplitude modulation, since at this frequency the skin depth in cadmium is large enough to allow penetration of the modulation into the entire sample.

The grid-leak detector built into the second stage of the marginal oscillator is sensitive to changes in rf power absorption, and thus to the real part of the surface impedance of the sample in the tank coil. An increase in the sample impedance leads to a positive voltage at the output of the detector, while a decrease produces a negative output. Thus the output of the detector of the oscillator was a 40-Hz sine wave whose amplitude was proportional to $\partial R/\partial H$, where R is the real part of the surface impedance. The output of the oscillator was amplified by a tuned amplifier (see Fig. 3) and then fed into a phase-sensitive detector. The dc output of the phase detector was applied to the Y axis of an

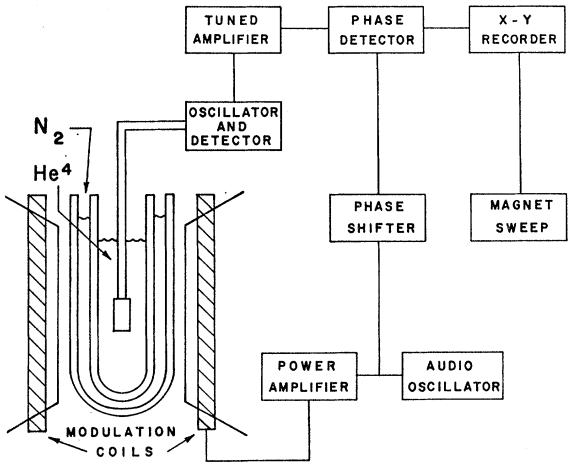

FIG. 3. Basic equipment diagram used in the RFSE.

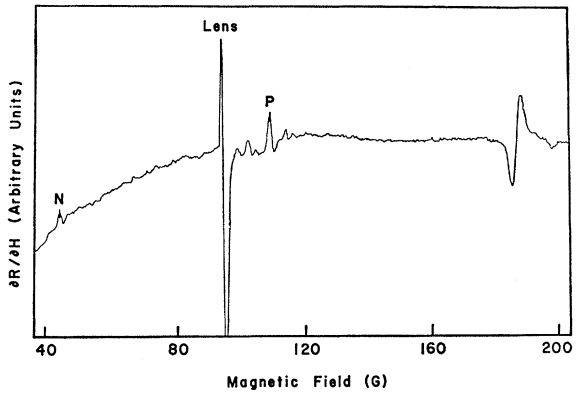

FIG. 4. Recorder trace for $\mathbf{n} \| [10\bar{1}0]$ obtained with H 46° from $[0001]$ in the $(10\bar{1}0)$ plane.

X-Y recorder whose X axis was set proportional to the applied magnetic field. The resulting plot was $\partial R/\partial H$ versus H.

IV. EXPERIMENTAL RESULTS

A. Data

The data for $\mathbf{n} \| [0001]$ were recorded by rotating the magnet in 1° steps over a 40° range that covered both axes, $[10\bar{1}0]$ and $[11\bar{2}0]$. The line shapes obtained from this orientation are discussed by Goodrich and Jones.[10]

Figure 4 shows a recorder trace for $\mathbf{n} \| [10\bar{1}0]$. The magnetic field is rotated from $[0001]$ to $[11\bar{2}0]$ in 1° and 2° steps. There are generally fewer size-effect peaks observed for this orientation than for the other two. The double-field "lens" peak is shown on this curve along with the primary lens peak and two other peaks. The lens peaks were observed to as high as fourth order, since in this case the orbits add at relatively flat portions of their trajectory. Their polarity seemed to invert for each successive occurrence, although the line shape becomes more complex and the amplitude decreases for the higher harmonics; thus their polarity is not easily determined.

A typical recorder trace obtained for $\mathbf{n} \| [11\bar{2}0]$ is shown in Fig. 5. A large number of peaks occurred with

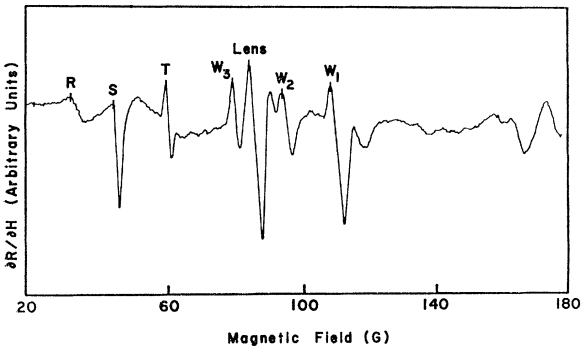

FIG. 5. Recorder trace for $\mathbf{n} \| [11\bar{2}0]$ obtained with H 50° from $[0001]$ in the $(11\bar{2}0)$ plane.

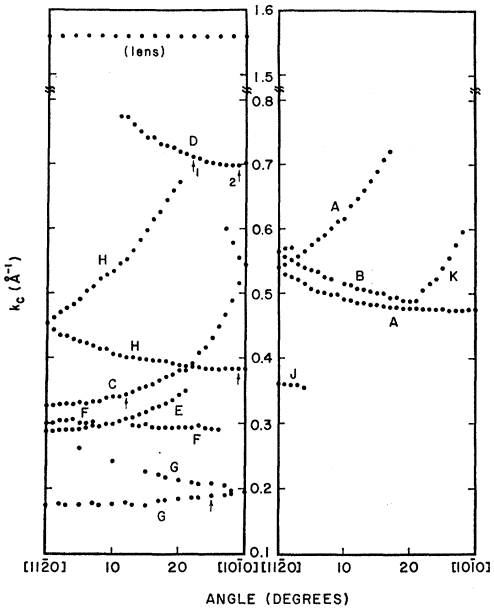

FIG. 6. Plot of experimental caliper k_c versus magnetic field direction for $\mathbf{n}\|[0001]$. The data are divided into (1) direct calipers and (2) orbit addition calipers. The arrows refer to Figs. 13 and 19.

considerable amplitude in this orientation. The primary and secondary lens peaks are shown along with several other peaks. The lens peak was again observed to as high as fourth order. No peak other than the lens was seen to exhibit the multiple-field behavior.

B. Determination of Critical Magnetic Fields and Calipers

There are several line shapes evident in Ref. 10 and in Figs. 4 and 5, most of which are considerably more complex than those predicted by Kaner and Fal'ko.[15] It is not always evident which of the several extremal points in the lines to choose as the critical magnetic field. Fukumoto and Strandberg[18] determined the shift

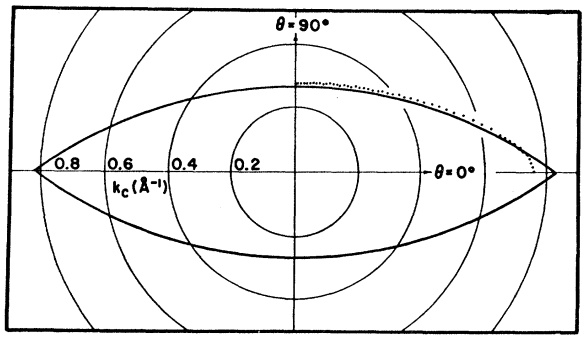

FIG. 7. Caliper values k_c obtained for the lens with $\mathbf{n}\|[10\bar{1}0]$. θ is the angle between **H** and [0001]. The magnetic field is rotated in the (10$\bar{1}$0) plane. The arcs represent the cross section of the single-OPW lens.

[18] A. Fukumoto and M. W. P. Strandberg, Phys. Letters **23**, 200 (1966).

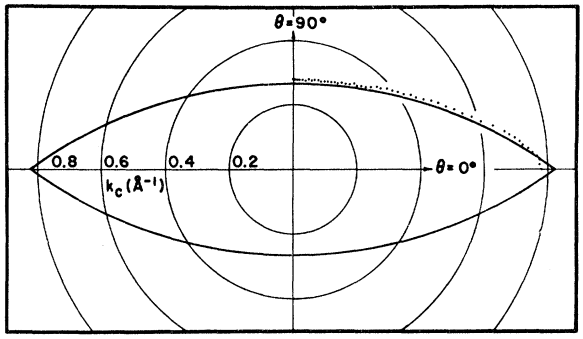

FIG. 8. Caliper values k_c obtained for the lens with $\mathbf{n}\|[11\bar{2}0]$. θ is the angle between **H** and [0001]. The magnetic field is rotated in the (11$\bar{2}$0) plane. The arcs represent the cross section of the single-OPW lens.

in magnetic field of various points in the line versus the applied frequency ω. They found that the lowest-field extremum in the curve $\partial R/\partial H$ versus H had a smaller ω dependence than any of the other points in the line, and thus concluded that this was the point to choose as the critical magnetic field. The same conclusion was reached in the present investigation by noting the change in line shapes due to changing the orientation of the coil relative to the sample axes and to the magnetic field. The low-field extremum had the only value of magnetic field that corresponded to an extremum for both coil orientations.

The critical magnetic fields were then converted into calipers by using Eq. (2). The experimental caliper values are plotted versus the direction of the applied magnetic field in Figs. 6–12. The data have been grouped into series by inspection of the recorder traces. Most of the individual series have been labeled with a Roman letter for reference.

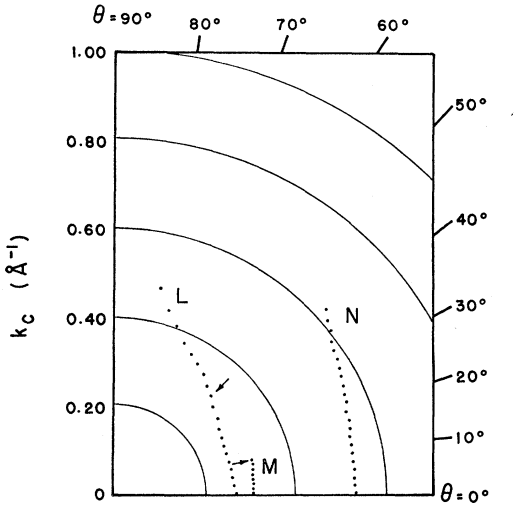

FIG. 9. Some of the caliper values k_c obtained with $\mathbf{n}\|[10\bar{1}0]$. θ is the angle between **H** and [0001]. The magnetic field is rotated in the (10$\bar{1}$0) plane.

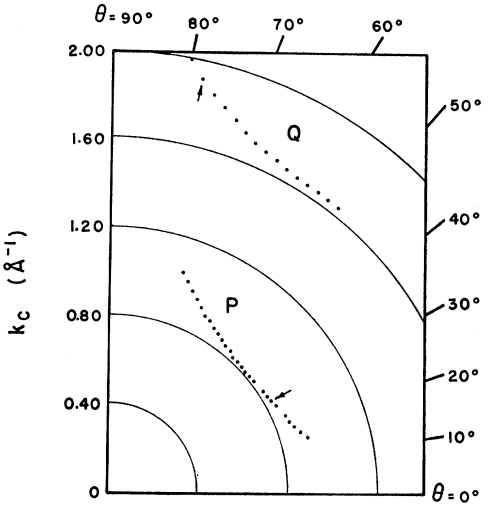

FIG. 10. Some of the caliper values k_c obtained with $\mathbf{n}\|[10\bar{1}0]$. θ is the angle between **H** and [0001]. The magnetic field is rotated in the $(10\bar{1}0)$ plane.

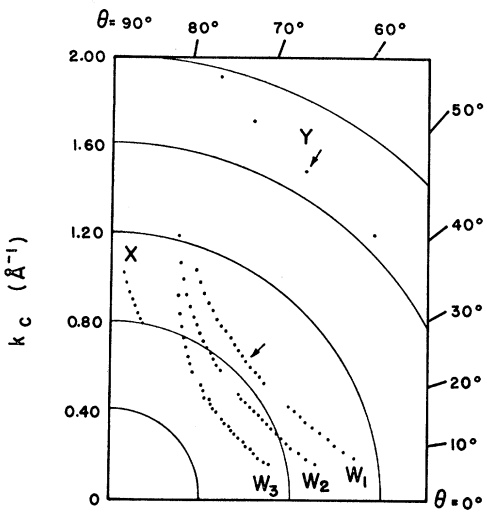

FIG. 12. Some of the caliper values k_c obtained with $\mathbf{n}\|[11\bar{2}0]$. θ is the angle between **H** and [0001]. The magnetic field is rotated in the $(11\bar{2}0)$ plane.

V. DATA ANALYSIS AND CALIPER ASSIGNMENT

In order to clarify the discussion below, two definitions are stated here. An "extremal orbit" is defined as an orbit on the FS in k space, the length of whose projection on a plane perpendicular to **n** is an extremum with respect to k_H (the component of **k** in the direction of **H**). An "extremal caliper" is defined as a vector quantity in k space which is in the direction of $\pm\mathbf{n}\times\mathbf{H}$ and has a magnitude equal to the length of the line segment formed by projecting an extremal orbit (in k space) onto a plane perpendicular to **n**. Thus an extremal caliper has a fixed magnitude and direction but is not fixed to any point in k space.

The RFSE obtains extremal calipers on the FS, and the term "caliper" will be used for this hereafter. The individual sheets of the FS and the assignment of the calipers to them are discussed in turn below.

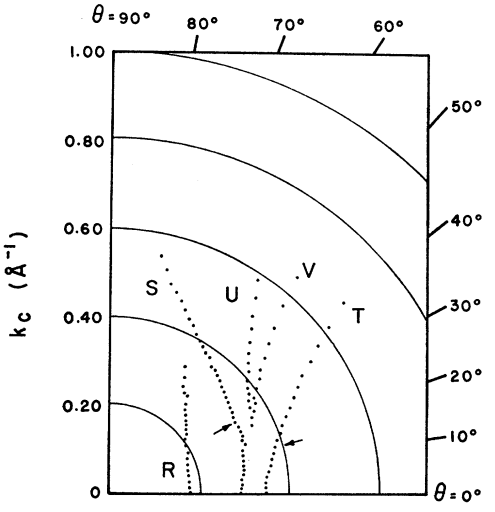

FIG. 11. Some of the caliper values k_c obtained with $\mathbf{n}\|[11\bar{2}0]$. θ is the angle between **H** and [0001]. The magnetic field is rotated in the $(11\bar{2}0)$ plane.

A. Third-Band Electron "Lens"

There was no difficulty in assigning particular calipers to the third-band electron surface called the "lens." The lens produced the most intense line observed for each orientation. With $\mathbf{n}\|[0001]$ the lens was seen to

TABLE I. Comparison of caliper values for the lens obtained by different sources.[a]

n,q[b] parallel to **H** parallel to Source	$[11\bar{2}0]$ $[0001]$	$[10\bar{1}0]$	$[10\bar{1}0]$ $[0001]$	$[11\bar{2}0]$	$[0001]$ $[10\bar{1}0]$	$[11\bar{2}0]$
Deaton[c]		0.550	1.556	0.550		
Daniel and Mackinnon[d]	1.458	0.54	1.428	0.498		
Gibbons and Falicov[e]	1.560	0.550		0.540		
Chang[f]	1.510	0.542	1.516	0.540		
Naberezhnykh *et al.*[g]	1.46	0.53	1.47	0.54		
Present investigation	1.563	0.599	1.516[h]	0.553	1.560	1.560
Free-electron values	1.658	0.540	1.658	0.540	1.658	1.658
Stark and Falicov[i]	1.508	0.541	1.508	0.541	1.508	1.508

[a] All calipers in Å^{-1}.
[b] Ultrasonic attenuation obtains the same calipers as the RFSE with **q**, the direction of sound propagation, in the same direction as **n**.
[c] B. C. Deaton, Ph.D. dissertation, The University of Texas, 1962 (unpublished).
[d] See Ref. 7.
[e] See Ref. 6.
[f] See Ref. 8.
[g] See Ref. 9.
[h] The line shape became rather complex as **H** neared [0001]; thus this result is subject to a larger error than the other values in this row. The same diameter is calipered with $\mathbf{n}\|[0001]$ and $\mathbf{H}\|[10\bar{1}0]$ and is considered more accurate.
[i] See Ref. 12.

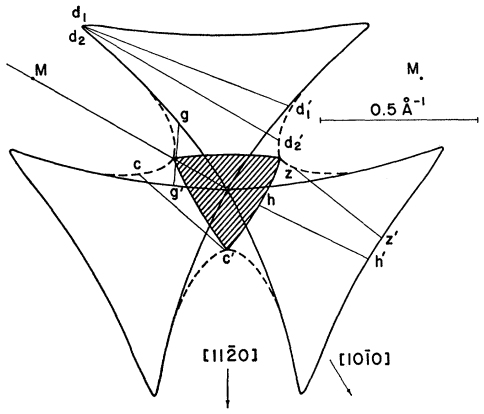

FIG. 13. Cross sections of second-band hole surface of cadmium consistent with present results and area data of Tsui and Stark (Ref. 3). The cross-hatched area is the AHL plane, the solid line is the ΓMK plane, and the dashed line represents the extremal size of the surface at points between the AHL and ΓMK planes. The representative calipers shown here are for the angles indicated by the arrows in Fig. 6.

have a circular cross section in the ΓMK plane[19] with diameter $k_c=1.560$ Å^{-1}, and this is plotted in Fig. 6. The lens calipers obtained from the $\mathbf{n}\|[10\bar{1}0]$ data lie in the ΓAHK plane and are given in Fig. 7, while the calipers obtained from the $\mathbf{n}\|[11\bar{2}0]$ data lie in the ΓALM plane and are plotted in Fig. 8. The arcs in Figs. 7 and 8 outline the single-OPW cross sections of the lens. The data are seen to agree quite well with the single-OPW predictions except near the edge of the lens where considerable rounding occurs. A summary of some of the most recent lens calipers is given in Table I. The diameters reported in this investigation are in reasonable agreement with the available ultrasonic data. The lens, however, is found to be quite smooth, with no bump at the center as reported by Gibbons and Falicov,[6] and no dip as observed by Chang.[8]

The cross-sectional areas of the lens could be computed from the formula for the area of an ellipse $S=\frac{1}{4}\pi k_1 k_2$, where k_1 and k_2 are the major and minor axes of the ellipse. From the data obtained with $\mathbf{n}\|[0001]$ the circular cross section in the ΓMK plane has an area of 1.911 Å^{-2}, and from the major diameters obtained with $\mathbf{n}\|[10\bar{1}0]$ and $\mathbf{n}\|[11\bar{2}0]$ the area is 1.861 Å^{-2}, both of which compare reasonably well with the value of 1.874 Å^{-2} obtained by Grassie.[2] The area of the elliptical cross section in the ΓAHK plane can be obtained with $\mathbf{n}\|[10\bar{1}0]$, and the ΓALM cross section can be computed using the $\mathbf{n}\|[11\bar{2}0]$ data. The results using the formula for the area of an ellipse are 0.658 and 0.686 Å^{-2}, respectively. However, direct measurements of these areas from Figs. 7 and 8 are equal within experimental error and give a value of 0.631 Å^{-2}, which is in fair agreement with Grassie's result[2] of 0.608 Å^{-2}.

[19] The previously published value of $k_c=1.5825$ Å^{-1} is in error because of incorrect selection of the critical magnetic field.

B. Second-Band Hole Surface

The second-band hole surface ("monster") consists of two trifoliate surfaces per BZ which are connected in the [0001] direction and which can be considered either inversion images of each other or mirror reflections of each other in the ΓAHK and ΓALM planes (see Figs. 1 and 2). The calipers obtained for these two surfaces with $\mathbf{n}$ parallel to one of the three principal directions ([0001], [10$\bar{1}$0], or [11$\bar{2}$0]) and $\mathbf{H}\perp\mathbf{n}$ are degenerate, and all the calipers for a given magnetic field direction are obtained by considering only one of the trifoliate surfaces (see Figs. 13–15). In Fig. 13 the large solid-line cloverleaf represents the ΓMK cross section ("waist") of the monster. The shaded portion represents the AHL cross section ("neck"), and the dashed lines indicate the extremities of the cross sections perpendicular to the hexagonal axis and intermediate to the ΓMK and AHL planes.

Because of the lack of inversion symmetry in each separate sheet of the second-band surface, the monster has no central calipers for $\mathbf{n}\|[0001]$ or $\mathbf{n}\|[10\bar{1}0]$, i.e., it has no series of calipers that have a common fixed

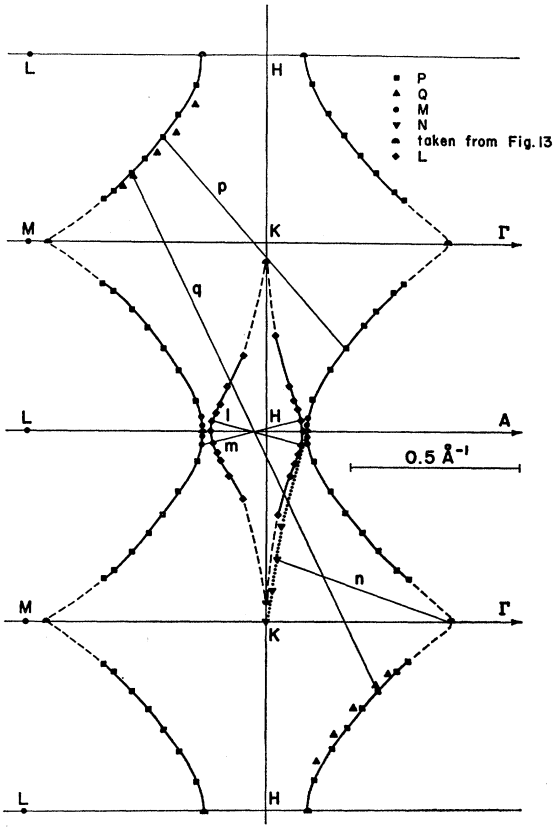

FIG. 14. ΓAHK cross sections of second-band hole surface (outer figure) and first-band hole surface (inner figure) consistent with present results. Dashed portion of first-band hole surface extrapolated to fit area data of Tsui and Stark (Ref. 3). Dashed portion of second-band surface interpolated to agree with Fig. 13 (see text). Representative calipers shown here are for the angles indicated by the arrows in Figs. 9 and 10.

point on a symmetry point or line in the BZ. Thus, while the direction of a caliper is known to be that of $\mathbf{n}\times\mathbf{H}$, there is no known point, line, or plane on which to fix the position of the caliper. This greatly complicates the determination of the FS from the extremal-caliper data.

The results of the energy-band calculation of SF were used to aid in the assignment of calipers to the second-band hole surface. Planar cross sections of the trifoliate structure parallel to the AHL and ΓMK planes were drawn from the values calculated by SF; the outline of this theoretical surface is that given in Fig. 16. Extremal calipers were measured from this construction and plotted versus angle of applied magnetic field with the results shown in Fig. 17. There are several types of extremal orbits to be considered. Figure 17(a) displays the open truncated orbit calipers. In Fig. 17(b) extremal orbits that have a true maximal or minimal extent for rotations in the [0001] plane are plotted. Figure 17(c) displays the closed orbits that are extremal by truncation, i.e., orbits in planes perpendicular to $\mathbf{H}$ that either increase or decrease in size until they reach

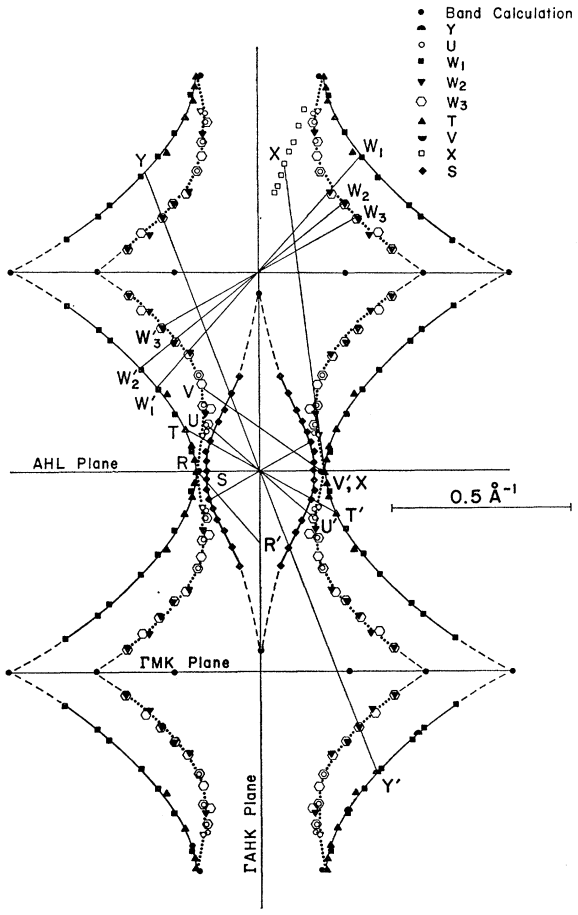

FIG. 15. Projections of extremal size of first- and second-band hole surfaces onto (11$\bar{2}$0) plane (see text). The representative calipers shown here are for the angles indicated in Figs. 11 and 12.

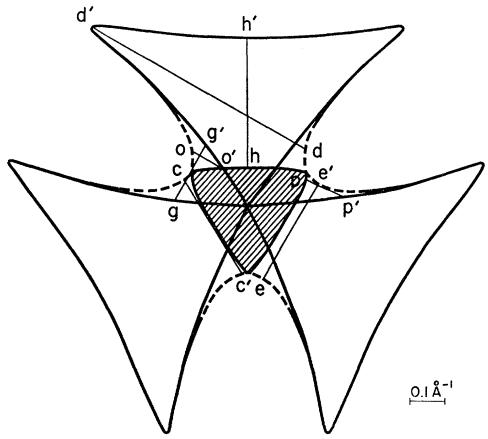

FIG. 16. Cross sections of the second-band hole surface of cadmium as obtained from the pseudopotential calculation of Stark and Falicov (Ref. 12). The cross-hatched area is the AHL plane, the solid line is the ΓMK plane, and the dashed line represents the extremal size of the surface at points between the AHL and ΓMK planes.

a point on the surface at which they no longer exist in the same form. The calipers zz′ and gg′ in Fig. 13 are two examples of truncated calipers. However, for the purposes of this experiment, calipers zz′ and gg′ have an entirely different nature. Caliper zz′ corresponds to an orbit whose truncation point (saddle point) lies within the skin depth of the sample when the magnetic field is such that the orbit reaches its critical size. Since the velocity of the carriers near the truncation point is nearly parallel to the applied magnetic field, they do not interact strongly with the applied electric field. Caliper gg′, on the other hand, is truncated at a point which does not lie within the skin depth at its critical size and thus can give rise to a size-effect peak. Of all of the truncated orbits with $\mathbf{H}$ in this plane only two are of this type: gg′ and cc′.

Open orbits existing on the second-band hole surface with $\mathbf{H}$ in the (0001) plane have their extremities perpendicular to [0001] in the AHL and ΓMK planes. Thus open orbits generated on this surface will caliper the difference in extent of the surface in these two planes. These orbits have a shape similar to the outline of the second-band surface in Fig. 14. The projection of the monster in the plane determined by two adjacent HK lines is shown in Fig. 14 along with the cross section of the "cap" in that plane which is enclosed by the monster. Calipers lying in this plane are obtained with $\mathbf{n}\|[10\bar{1}0]$. The principal calipers obtained with $\mathbf{n}\|[11\bar{2}0]$ for the monster and the cap are central in the sense that there exists a symmetry line in the BZ through which all of the calipers in a given series have their midpoints. These lines are either the ΓK or the AH lines (these lines are normal to the page in Fig. 15). Since these calipers are not fixed to a single point on these lines, the calipers obtained do not all lie in the same plane.

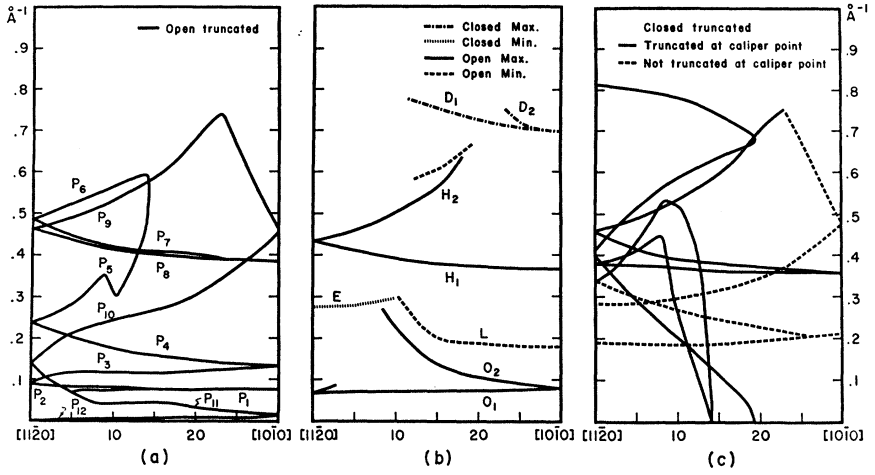

FIG. 17. Caliper values obtained from the second-band hole surface of Stark and Falicov (Ref. 12) and shown in Fig. 16. See text for discussion.

Calipers series labeled C, D, G, H, M, N, P, Q, R, T, U, V, W_1, W_2, W_3, X, and Y are assigned to definite orbits on the second-band hole surface. Representative calipers for each of these are shown by lines labeled with the corresponding small letters in Figs. 13–15.

Series C, M, P, Q, T, W_1, and Y are minimum calipers arising from closed orbits. Inspection of the series P and Q in Fig. 10 leads naturally to the assignment of P to the waist orbit and Q to the extended waist orbit (see Fig. 14). Assignment of series M to the neck orbit then follows. Similarly, the assignments of W_1 and Y in Fig. 12 to the waist orbit and the extended waist orbit for $\mathbf{n}\|[11\bar{2}0]$ is immediate (see Fig. 15). Series T (Fig. 11) is easily seen to be due to the minimal neck caliper (see Fig. 15).

Maximum caliper series D results from closed orbits around the arms of the monster. Series H is due to minimal open orbits moving parallel to [0001]. The caliper values obtained for both the D and H series for the magnetic field along $[10\bar{1}0]$ agree with the dimensions given by SF to within 1%.

With **H** lying within about 10° of the basal plane, closed orbits lying in the concave portion of the monster can exist. Series G and X arise from truncation of these orbits. No series comparable with series X was observed for $\mathbf{n}\|[10\bar{1}0]$. This is probably because truncation of such an orbit would occur at the caliper point and there are no data observed in this experiment that can be attributed to an orbit truncated in this way. Series X is truncated slightly off one of its caliper points.

Series N, U, V, W_2, and W_3 arise from broken orbits of a type discussed by Gantmakher.[20] The calipers arise when the carriers pass through the skin layer on each side of the sample and are later scattered by the sample surface. Figure 18 shows some of these types of orbits. Series R fits the orbit shown in Fig. 18(c). This series calipers from the ΓAHK plane to the vertex of the AHL cross section of the monster. This caliper provides little useful information about the shape of the surface.

Table II summarizes the assignments of the calipers obtained for the monster with $\mathbf{H}\|[0001]$. The assignments given here differ from those given previously by Goodrich and Jones[10] and the differences are due mainly to the assignment of the H series of calipers to the minimum open orbit rather than the previously assigned A series. Five of the calipers were assigned to orbit additions where two orbit diameters add to span the sample thickness. The minimum open orbit oo′ as indicated in the theoretical surface, Fig. 17, was observed indirectly through orbit addition. It was not observed directly because it would occur at very low values of the applied magnetic field where the rapidly changing surface impedance obscures the size-effect peaks. The series I was unassigned and may have been structure on the much more intense series C.

Three views of the second-band hole surface, Figs. 13–15, were constructed in final form after the assignments of the caliper series had been made. First the AHL cross section (triangular portion of Fig. 13) was constructed by using its dimension in the $[10\bar{1}0]$ and $[11\bar{2}0]$ directions (series T and M with $\mathbf{H}\|[0001]$, re-

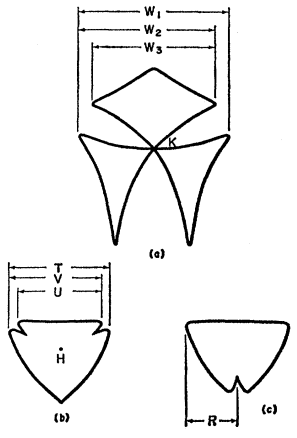

FIG. 18. Examples of some of the broken orbits observed with $\mathbf{n}\|[11\bar{2}0]$: (a) waist orbits, (b) neck orbits, and (c) a near neck orbit calipered at a turning point.

[20] V. F. Gantmakher and I. P. Krylov, Zh. Eksperim. i Teor. Fiz. 49, 1054 (1965) [English transl.: Soviet Phys.—JETP 22, 734 (1966)].

TABLE II. Caliper assignments to second-band orbits for field rotations in the (0001) plane.

Description	Experimental curve[a]	Theoretical surface[b]	Theoretical curve[c]
Min open orbit	H	hh′	H
Min open orbit	Not observed	oo′	O
Max closed orbit	D	dd′	D
Orbit addition	E	oo′+gg′	O+G
Truncated orbit	G	gg′	G;L
Min closed orbit	C	cc′	C
Orbit addition	A	oo′+hh′	O_1+H
Orbit addition	K	oo′+cc′	O_2+C
Orbit addition	B	pp′+hh′	P_2+H
Orbit addition	J	ee′+oo′	E+O

[a] See Fig. 6.
[b] See Fig. 16.
[c] See Fig. 17.

spectively) together with the known cross-sectional area.[3] A mild constraint was provided by the fact that the first-band hole calipers (series F) had to fit within this cross section.

Because of the nature of the magnetic breakdown at the point K observed by Tsui and Stark,[3] it is known that this surface passes very near to the point K. Thus with **H**‖[0001], series N (Figs. 9 and 14) provided the extent of the monster in the [11$\bar{2}$0] direction of the ΓMK plane from the $\Gamma K\Gamma$ line. This provides a critical dimension in Figs. 13 and 14. The principal open orbit, series H, was then used to construct the outer portion of the ΓMK cross section (large solid cloverleaf). Series C, the minimum closed orbit, and series D, the maximum closed orbit, were then used together to construct the outline of the cross sections intermediate to the ΓMK and AHL planes (dashed portion of Fig. 13). The concave inner portion of the ΓMK cross section was determined from the truncated caliper series G. After extrapolating the uncalipered segments of the ΓMK cross section, its area was measured and found to agree with the results of Tsui and Stark.[3]

Figure 14 was constructed primarily from data obtained with **n**‖[10$\bar{1}$0]. The dimensions in the ΓMK and AHL planes were taken from Fig. 13. Series M, the minimum neck caliper, series P, the minimum waist caliper, and series O, the minimum extended waist caliper, were used together to determine this outline of the monster. For **H** near [0001], series Q deviated somewhat from this figure. Since the linewidth in RFSE is roughly proportional to the magnitude of the magnetic field at which it occurs, series Q, having larger values than series P, would be subject to a larger error than would series P. Thus series P was used in these regions. Series N is shown plotted so as to keep one end fixed in the ΓMK plane.

Figure 15 was obtained by plotting the data obtained with **n**‖[11$\bar{2}$0]. Since all of the principal calipers obtained in this orientation were central, the outline of the monster could be obtained by plotting the half-calipers in polar form. Series W_2 is not central, but it provides no information other than a consistency check. Series V, X, and R are plotted keeping one end of the caliper fixed in the AHL plane. The solid-line figure that results is a shadowgram, or projection of the external size of the second-band hole surface onto a (11$\bar{2}$0) plane, and the dotted outline is a shadowgram of one arm of the monster onto this plane.

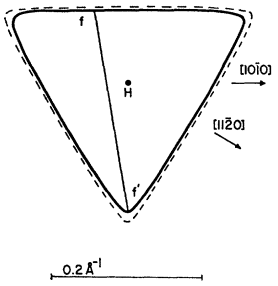

FIG. 19. AHL cross section of first-band hole surface of cadmium consistent with the present results and the area data of Tsui and Stark (Ref. 3). The dashed line represents the cross section of the second-band hole surface in the AHL plane.

The solid and dotted lines in Figs. 14 and 15 have been determined by at least one series of calipers. The tips on the monster arms were determined from Fig. 13, and the dashed lines represent interpolated points. All the calipers in the region of overlap in Figs. 13–15 were found to agree within experimental accuracy.

C. First-Band Hole Surface

The first-band hole surface (cap) consists of two sections per BZ centered at the point H; each sheet has threefold symmetry about [0001]. This surface has the same symmetry properties as the second-band hole surface discussed previously; thus all the calipers for this surface can be obtained by considering only one of the two sections.

In Fig. 19 the AHL cross section of the cap is shown as the solid figure within the second-band neck (dashed figure). The ΓAHK cross section is shown within the second-band cross section in Fig. 14. The same remarks stated above for calipers obtained with **n**‖[11$\bar{2}$0] on the second-band hole surface are also valid for the first-zone hole surface. Thus the extremal calipers obtained for the cap with **n**‖[1120] do not all lie in a plane, and the outline in Fig. 15 is not a true cross section of the cap, but a shadowgram.

The caliper series labeled F, L, and S have been assigned to the first-band hole surface. The representative calipers shown in Figs. 14, 15, and 19 are for the angles indicated by the arrows in Figs. 6, 9, and 11. The assignments of L and S to the cap are quite natural considering the assignment of M and T to the neck of the second band (see Figs. 9, 11, 14, and 15). The assignment of F arose from the assignment of L, since the same caliper is obtained with **H**‖[10$\bar{1}$0] for **n**‖[0001] and with **H**‖[0001] for **n**‖[10$\bar{1}$0]. The AHL cross section shown in Fig. 19 and the ΓAHK cross section, Fig. 14, were obtained using the previously described self-consistent method with the known areas of 0.063 Å^{-2} for the AHL cross section and 0.105 Å^{-2} for the ΓAHK cross section as determined from the dHvA data.[3] The dashed portion

of the ΓAHK cross section shown in Fig. 14 was extrapolated to give the correct areas. No similar extrapolation was possible for the section shown in Fig. 15 because here the calipers do not trace out the maximum area orbit on the cap obtained with $\mathbf{H}\|[11\bar{2}0]$.

VI. CONCLUSIONS

The results obtained in this experiment show very good agreement with the nonlocal pseudopotential calculation of Stark and Falicov.[12] Although this calculation was performed by adjusting the pseudopotential coefficients to give the correct areas of the various sections of the FS, the present results show that agreement with detailed dimensions is also obtained. In some directions the calipers agree within 1% and all of the general features of the calculated surface are found. All of the calipers that are found can be assigned to orbits on the first-, second-, and one section of the third-band sections of the FS. Thus the third-band electron stars and the forth-band electron cigars are found to be absent, i.e., the corresponding energy levels are above the Fermi level. This conclusion is further supported by the fact that the size of the first- and second-band hole surfaces are such that in order to obtain the correct number of electrons, the volume occupied by electrons in the third and fourth bands cannot be larger than that included in the lens alone.

A summary of the comparison between theory and experiment is presented in Table III, which also lists various dimensions of the FS and some of the separations between different sheets. The theoretical values correspond to the calculation of Stark and Falicov.[12] The agreement is, in general, very good.

A final word about line shapes is in order. The line associated with the lens in Fig. 4 is similar to that predicted by Kaner and Fal'ko[15] for a maximum, but the line labeled T in Fig. 5 is quite different from that predicted for a minimum caliper; yet it is easy to see from Fig. 11 that it must be assigned to the minimum neck orbit. Furthermore, the line labeled S in Fig. 5 is similar to the predicted minimum orbit shape, but inspection of Fig. 11 shows it to arise from the maximum caliper on the cap.

TABLE III. Dimensions of the FS. All dimensions in Å^{-1}.

	Expt.	Theory
Lens		
From Γ in ΓA direction	0.276	0.271
From Γ in ΓK direction	0.780	0.754
From Γ in ΓM direction	0.780	0.754
Second-zone holes		
From K in $K\Gamma$ direction	0.494	0.491
From H in HA direction	0.112	0.114
From H in HL direction	0.192	0.180
First-zone holes		
From H in HA direction	0.108	0.110
From H in HL direction	0.178	0.168
From H in HK direction		0.505
Between first-zone holes and second-band holes in AHL plane		
Along HA direction	0.004	0.004
Along HL direction	0.014	0.013
Between arms of the second-band hole surfaces in ΓMK plane		
Parallel to MK direction		0.054

ACKNOWLEDGMENTS

The authors are indebted to Professor C. G. Grenier for many informative discussions. One of the authors (R.C.J.) wishes to thank the U. S. Department of Health, Education, and Welfare for its support in the form of a fellowship, and the Dr. Charles E. Coates Memorial Fund of the L. S. U. Foundation (donated by George H. Coates) for financial assistance in the preparation of this manuscript.